Acta Pharmaceutica Sinica B 2024;14(3):1412−1427

Chinese Pharmaceutical Association
Institute of Materia Medica, Chinese Academy of Medical Sciences

Acta Pharmaceutica Sinica B

www.elsevier.com/locate/apsb
www.sciencedirect.com

ORIGINAL ARTICLE

Bioorthogonal microglia-inspired mesenchymal stem cell bioengineering system creates livable niches for enhancing ischemic stroke recovery *via* the hormesis

Jianpei Xu[a,b], Yinzhe Sun[a,b], Yang You[a,b], Yuwen Zhang[e], Dan Huang[f], Songlei Zhou[a,b], Yipu Liu[a,b], Shiqiang Tong[a,b], Fenfen Ma[a,b], Qingxiang Song[c], Chengxiang Dai[g,h], Suke Li[g,h], Jigang Lei[g,h], Zhihua Wang[d,*], Xiaoling Gao[c,*], Jun Chen[a,b,*]

[a]*Shanghai Pudong Hospital & Department of Pharmaceutics, School of Pharmacy, Fudan University, Shanghai 201203, China*
[b]*Key Laboratory of Smart Drug Delivery, Ministry of Education, School of Pharmacy, Fudan University, Shanghai 201203, China*
[c]*Department of Pharmacology and Chemical Biology, State Key Laboratory of Oncogenes and Related Genes, Shanghai Universities Collaborative Innovation Center for Translational Medicine, Shanghai Jiao Tong University School of Medicine, Shanghai 200025, China*
[d]*Department of Emergency, Shanghai Pudong Hospital, Fudan University Pudong Medical Center, Shanghai 201399, China*
[e]*Institute of Science and Technology for Brain-Inspired Intelligence & Department of Neurology, Fudan University, Shanghai 201203, China*
[f]*Department of Rehabilitation Medicine, Huashan Hospital, Fudan University, Shanghai 201203, China*
[g]*Daxing Research Institute, University of Science and Technology Beijing, Biomedical Industry Base, Zhongguancun Science and Technology Park, Beijing 102600, China*
[h]*Cellular Biomedicine Group Inc., Shanghai 201210, China*

Received 2 July 2023; received in revised form 11 September 2023; accepted 28 September 2023

*Corresponding authors.
E-mail addresses: wzhys@163.com (Zhihua Wang), shellygao1@sjtu.edu.cn (Xiaoling Gao), chenjun@fudan.edu.cn (Jun Chen).
Peer review under the responsibility of Chinese Pharmaceutical Association and Institute of Materia Medica, Chinese Academy of Medical Sciences.

https://doi.org/10.1016/j.apsb.2023.11.009

KEY WORDS

Ischemic stroke;
Mesenchymal stem cell;
Cell engineering;
Hormesis effect;
Bioorthogonal chemistry;
Microglia;
Reactive oxygen spices;
Proinflammatory cytokines

Abstract Mesenchymal stem cells (MSCs) experience substantial viability issues in the stroke infarct region, limiting their therapeutic efficacy and clinical translation. High levels of deadly reactive oxygen radicals (ROS) and proinflammatory cytokines (PC) in the infarct milieu kill transplanted MSCs, whereas low levels of beneficial ROS and PC stimulate and improve engrafted MSCs' viability. Based on the intrinsic hormesis effects in cellular biology, we built a microglia-inspired MSC bioengineering system to transform detrimental high-level ROS and PC into vitality enhancers for strengthening MSC therapy. This system is achieved by bioorthogonally arming metabolic glycoengineered MSCs with microglial membrane-coated nanoparticles and an antioxidative extracellular protective layer. In this system, extracellular ROS-scavenging and PC-absorbing layers effectively buffer the deleterious effects and establish a micro-livable niche at the level of a single MSC for transplantation. Meanwhile, the infarct's inanimate milieu is transformed at the tissue level into a new living niche to facilitate healing. The engineered MSCs achieved viability five times higher than natural MSCs at seven days after transplantation and exhibited a superior therapeutic effect for stroke recovery up to 28 days. This vitality-augmented system demonstrates the potential to accelerate the clinical translation of MSC treatment and boost stroke recovery.

1. Introduction

Mesenchymal stem cells (MSCs) show promising potential in stroke treatment, especially in neuroprotection and neurological recovery[1−4]. Distinguished from conventional drug therapy, MSCs are more comprehensive in treating stroke injuries, such as alleviating excessive inflammation in the acute phase, remodeling the infarct's harsh microenvironment, and augmenting endogenous repair progress[5,6]. However, the clinical outcomes of MSC therapy in ischemic stroke treatment are vastly differentiated, resulting in a contentious therapeutic mechanism and impeding the clinical translation of the therapy. The most problematic aspect of this challenge is that MSCs' therapeutic potential is severely constrained by their fragile vitality in the complicated and inhospitable milieu of brain infarction. Consequently, it is necessary to build a bioengineering system to improve the vitality of MSCs to boost stroke recovery and obtain consistent clinical results.

Reactive oxygen species (ROS) and proinflammatory cytokines (PC) are crucial bidirectional mediators in stroke pathological and self-healing development, depending on their endogenous level[7]. In the acute phase after ischemic reperfusion injury, apoptosis-clearance progress dominates the infarct core, producing excessive cytotoxic ROS and PC (high dose level) to kill the injured cells and create an uninhabitable microenvironment[8−13]. While in the chronic phase, self-healing progress is dominant. Moderate ROS and PC (low dose level) are key neuroprotective signaling factors that activate endogenous stem cells and microglia to inhibit inflammation and promote recovery[7,14]. This hormesis effect poses a great threat to traditional stroke treatment but brings dawn for MSC therapy[15]. Flexible hormesis response is an inherent mechanism operative in the purposive fixity of cellular resilience and survival, that stressors are beneficial at a low level but harmful at a high level[16−19]. Therefore, converting the ROS and PC in the infarct core from high cytotoxic level into low beneficial level may provide a promising approach to reverse transplanted MSCs' vitality dilemma and improve their therapeutic effects. However, there is currently no effective strategy capable of achieving this hormesis conversion to improve MSC therapy for stroke treatment.

Biomimetic "cellular surface arming" strategy based on bioorthogonal cellular engineering exhibits promising potential to protect and enhance the transplanted MSCs' vitality in infarct brain *via* hormesis effect[10,20−22]. Based on this "cellular surface arming" strategy, we proposed the design of a novel MSCs engineering approach to introduce a biomimetic ROS and PC buffering layer to utilize the hormesis effect and concrete livable niches, not only for enhancing MSCs viability but also for remodeling microenvironment and augmenting endogenous recovery. Inspired by the inflammatory modulator role of microglia *via* PC-receptor mode in ischemic stroke, we supposed that the microglia derived membrane could absorb excessive PC by its abundant PC receptors. As the brain's resident macrophages, microglia are the principal immune cells and are involved in stroke injury[23]. They are highly active in a resting state and continually monitor the surrounding microenvironment[24]. Upon the brain ischemic injury, abnormal ROS and PC rapidly activate microglia and lead to the following immune cascade[25,26]. In addition to PC absorption, lipoic acid (LA), a highly efficient natural antioxidant, was chosen as the crucial extracellular antioxidative scavenger[27,28]. After the PC absorption and ROS scavenging, high cytotoxic level ROS and PC could be buffered to low beneficial level, constructing a livable micro-niche at the level of a single MSC for transplanted MSCs to enhance their biological activity. Moreover, at the tissue level, the inanimate infarct core could be remodeled to another livable niche for recovery progress.

Here, we developed the microglia inspired MSC bioengineering system in a modular assembly mode by biomimetic nanotechnology and bioorthogonal chemistry (Scheme 1A)[29−33]. Firstly, the azide-MSC module (MSC-N_3) was prepared *via* metabolic glycoengineering[34−36]. The PC absorbing module (HM-NP) was fabricated by the activated HAPI microglia derived membrane (HM) coating poly (lactic-*co*-glycolic acid) nanoparticle (NP). After insertion of bioorthogonal linker dibenzylcyclooctyne (DBCO)-PEG-DSPE, DBCO-HM-NPs could be covalently decorated on azide-MSC module to get DBCO-HM-NP-MSC. Finally, the antioxidative module (LA-PEG-N_3) was armed on DBCO-HM-NP-MSC *via* the same bioorthogonal method to achieve the dual-protection MSC bioengineering

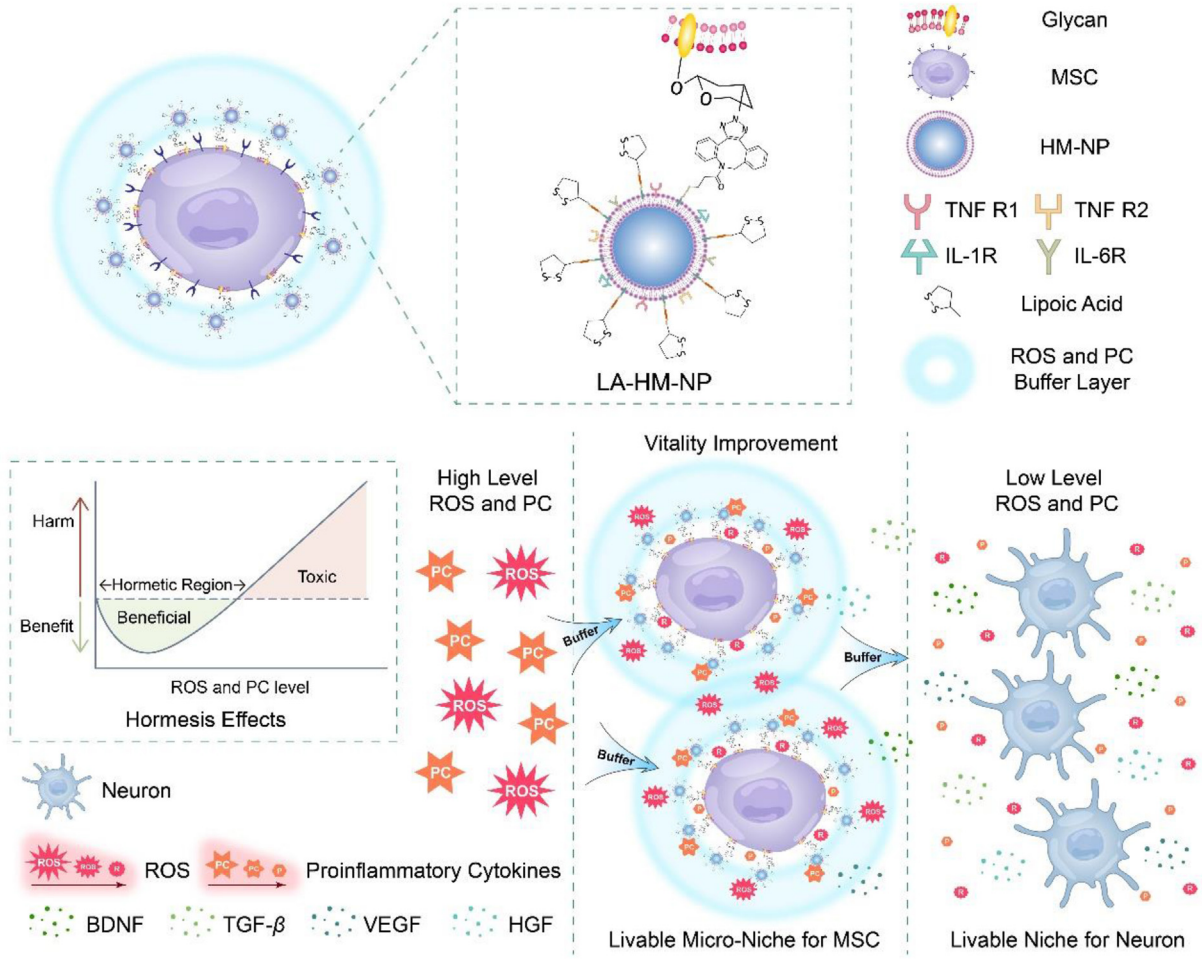

Scheme 1 Bioorthogonally surface-armed MSCs construct livable niches for augmenting ischemic stroke recovery *via* the hormesis effect. (A) A dual buffer layer (ROS and PC) constructed by lipoic acid decorated microglia membrane coating nanoparticles (LA-HM-NPs) armed on metabolic glycoengineered MSC bioorthogonally to prepare the LA-HM-NP-MSC. (B) When LA-HM-NP-MSCs migrated to the infarct area, the ROS and PC dual-buffering layer could effectively scavenge the overproduced ROS and PC by the lipoic acid and HAPI-derived membrane, and convert their effects on MSCs and neurons from high harmful level to low beneficial level. Firstly, the surface arming on engineered MSCs could decrease the excessive ROS and PC, buffer them to be beneficial factors around single MSC, and create a micro-livable niche at the level of a single MSC. Then at the tissue level, the infarct's inanimate milieu was transformed into a new living niche with low beneficial level ROS and PC, to facilitate endogenous healing *via* modulating the hormesis effect. This system not only improves transplanted MSCs' vitality and bioactivity but also protect neuron to avoid further stroke injuries.

system (LA-HM-NP-MSC). Benefiting from this "cellular surface arming" strategy (Scheme 1B), LA-HM-NP-MSCs show great resistance against high cytotoxic level ROS and PC, and their therapeutic activity was enhanced significantly *via* the controllable hormesis effect. Upon LA-HM-NP-MSCs migrated to the infarct area, the ROS, and PC dual-buffering layer could effectively scavenge the overproduced ROS and PC by the lipoic acid and HAPI derived membrane, and convert their effects on MSCs and neurons from high harmful level to low beneficial level. Firstly, the surface arming on engineered MSCs could decrease the excessive ROS and PC, buffer them to be beneficial factors around single MSC, and create a micro-livable niche at the level of a single MSC. Then at the tissue level, the infarct's inanimate milieu was transformed into a new living niche with low beneficial level ROS and PC, to facilitate endogenous healing *via* modulating the hormesis effect. Analyzing from data, the viability of intravenously transplanted MSCs was increased 5-fold than natural MSCs *in vivo*. Moreover, on Day 28 after transplantation, LA-HM-NP-MSCs still exhibited valid anti-stroke effects, while the natural MSCs treated group showed worse outcomes. In all, this bioengineering system integrated protection and enhancement for MSCs, and effectively buffers the deleterious effects to beneficial effects. It constructed livable niches for enhancing ischemic stroke recovery *via* the hormesis effect and would provide a new approach for improving MSC therapy and accelerate its clinical translation.

2. Materials and methods

2.1. *Materials*

Poly (D,L-lactide-*co*-glycolide) COOH (IV = 0.55−0.65, 75/25) was purchased from Xi'an Ruixi Biotechnology Co. (Xi'an, China). DSPE-PEG_{2000}-DBCO and NH_2-PEG_{2000}-N_3 were purchased from AVT (Shanghai, China) Pharmaceutical Tech Co.,

Ltd. Ac4GalNAz (catalog number 1086-100) were purchased from Click Chemistry Tools (Scottsdale, USA). *In vitro* adipogenesis differentiation kit, *in vitro* osteogenesis differentiation kit and *in vitro* chondrogenesis differentiation kit were purchased from Chembio-engine (Shanghai, China). The hydrogen peroxide assay kit (catalog: S0038), Reactive oxygen species test kit (catalog: S0033S), and BeyoClick EdU assay kit (catalog: C0078L) were obtained from Beyotime Biotechnology (Shanghai, China). Rat TNF-α ELISA kit, rat IL-1β ELISA kit, and rat IL-6 ELISA kit were obtained from Shanghai Epizyme Biomedical Technology (Shanghai, China). Anti-NeuN antibody (catalog: ab177487) was obtained from Abcam (Shanghai, China). The other chemical reagents were obtained from Sinopharm Chemical Reagent Co. (Shanghai, China). Refrigerated centrifuge (Biofuge Stratos, Thermo, MA, USA).

All animals were treated in accordance with the Guide for the Care and Use of Laboratory Animals, approved by the Institutional Animal Care and Use Committee of Fudan University (approval number 2020-09-YJ-CJ-01).

2.2. Isolation of HAPI microglia membrane

4×10^8 (2×10^7 cells/mL, 20 mL) LPS (10 ng/mL) stimulated-HAPI cells were suspended in ice-cold TM buffer solution (10 mmol/L Tris + 1 mmol/L $MgCl_2$, pH = 7.4) added with protease inhibitors. After 6 times freeze-thawing process, the cells were homogenized in an ice bath. Then the solution was centrifuged for 15 min (4 °C, 2000×*g*). The upper supernatant was preserved for further centrifugation for an additional 25 min (4 °C, 11,500×*g*). The resulting supernatant was collected again for ultrahigh-speed centrifugation for 1 h (4 °C, 100,000×*g*). Finally, ultrapure water was used to resuspend the precipitation and HAPI vehicles were obtained. HAPI vehicles were stored at −80 °C for further study.

2.3. Preparation of DBCO-HM-NP

HAPI vehicles were sonicated at 200 Watt for 5 cycles in ice immersion to get the membrane fragments. Then the membrane fragments were mixed with NP at different membrane/PLGA weight ratios (0.005, 0.01, 0.02, 0.05, 0.08, 0.1, 0.2, 0.5, 0.8, 1.0, and 2.0). Sample HAPI membrane was lyophilized to weigh and calculate the weight of the membrane. The combinations were then sonicated in an ice-bath ultrasound instrument for about 3−5 min, and then were centrifuged for 20 min (4 °C, 11,500×*g*) to remove redundant membrane in the supernatant and collected the purified HM-NP in the precipitation. DSPE-PEG_{2000}-DBCO was dissolved in deionized water and then added into the HM-NP solution at the 0.5 weight ratio (DSPE-PEG_{2000}-DBCO/PLGA) for stirring 2 h in an ice bath. The combination was then centrifuged for 20 min (4 °C, 11,500×*g*) to remove redundant DSPE-PEG_{2000}-DBCO in the supernatant and collected the purified DBCO-HM-NP in the precipitation. The surface ζ potential and hydrodynamic size were detected by dynamic light scattering (DLS) (Zetasizer Nano-ZS, Malvern 3600, Worcestershire, UK).

2.4. Preparation of LA-HM-NP-MSC

MSCs were cultivated to 65%−75% cell confluence. Refreshing the medium with 50 μmol/L Ac4GalNAz contained medium. MSCs were cultivated in common conditions (5% CO_2, 37 °C) for approximately 72 h to get N_3-MSC. A moderate amount of DBCO-HM-NP was suspended in the medium to obtain a concentration of 500 μg/mL. The sample nanoparticle suspension was lyophilized to weigh the weight and calculate the concentration of the DBCO-HM-NP. Then, add the combination above to the washed N_3-MSC for co-cultivation for about 3 h, and wash with Dulbecco's phosphate buffered saline (D-PBS) 5 times to get the prepared DBCO-HM-NP-MSC. Moderate amounts of LA-PEG_{2000}-N_3 were added into the medium to obtain a concentration of 500 μg/mL. And the special medium above was added to DBCO-HM-NP-MSC for co-cultivation for about 3 h. Finally, remove the upper medium and wash the MSCs with D-PBS 5 times to obtain the LA-HM-NP-MSCs.

2.5. Preparation of proinflammatory cocktails

Equivalent amounts of TNF-α, IL-1β, and IL-6 were mixed at the same concentration in the culture medium without FBS. For example, 1 ng/mL proinflammatory cocktail is the basic medium that contains 1 ng/mL TNF-α, 1 ng/mL IL-1β, and 1 ng/mL IL-6.

2.6. Conditioned medium from proinflammatory cocktail stimulated HAPI microglia

Culturing HAPI to 80%−90% cell confluence in a culture flask. Then, refreshing the common culture medium with different proinflammatory cocktail-contained mediums and co-culturing for 24 h to obtain the conditioned mediums.

2.7. Proinflammatory cytokines (PC) buffer assay

10×10^4 cells/pore HAPI were seeded and cultured in the 6-well plate in ordinary condition until the cell confluence was up to 80%−90%. Tilting the pipette at a 45-degree angle and pressing it against the bottom left of the 6-well plate, then injecting 2 mL PC medium into the plate at a speed of 200 μL/s. 10 min later, the tested cells were treated with 4% polyformaldehyde solution for 15 min and the nucleus were dyed *via* Hoechst 33342. Then, the cell morphology was recorded by fluorescence microscope.

2.8. In vitro *antioxidation assay*

The 6×10^3 cells/pore MSCs were seeded and stabilized in a 96-well plate in a 37 °C, 5% CO_2 incubator for about 1 day. MSCs for engineering were treated with Ac4GalNAz (50 μmol/L) for about 3 days and then co-cultivated with DBCO-HM-NP combination, HM-NP combination, or NP combination for 2 h. A moderate amount of LA-PEG_{2000}-N_3 (500 μg/mL) dissolved in the medium were co-cultivated with various MSC group. After the engineering process, various MSC groups were treated with 100 μmol/L H_2O_2 in HBSS for 2 h, then renewed the HBSS with a common medium for another 1 day. Then the MSC vitality was detected by the MTT assay kit.

For the H_2O_2 elimination assay, 2×10^5 cells/pore MSCs were seeded and stabilized in a 6-well plate in a 37 °C, 5% CO_2 incubator for about 1 day. MSCs for engineering were treated with Ac4GalNAz (50 μmol/L) for about 3 days and then co-cultivated with DBCO-HM-NP combination or HM-NP combination for 2 h. LA-PEG_{2000}-N_3 (500 μg/mL) dissolved in Medium were co-cultivated with various MSC groups. After the engineering process, various MSC groups were treated with 100 μmol/L H_2O_2 in HBSS for 2 h. 200 μL HBSS samples were collected for detection

at each preset time. A hydrogen peroxide assay kit was used to detect the H_2O_2 concentration.

2.9. *In vivo NIRF imaging tracking of intravenously transplanted MSC*

2×10^6 MSCs of various groups (20%, 50%, 100%, MSC) were suspended in 1 mL precooled PBS (pH 7.4). Then, the cell suspension prepared above was injected into the MCAO rats *via* vein within 2 h upon the model being constructed. According to the present time, living tested rats and their *ex vivo* brains were scanned respectively. ImageStreamX MarkII system (Merck, Darmstadt, Germany) was used for the NIRF signals record. Region-of-interest (ROI) analysis was used for quantifying the NIRF intensity.

2.10. *T_2-weighted MRI*

An 11.7 T animal MR system (Bruker BioSpec, 11.7/16USR, Germany) was used to record T_2-weighted MR signals according to preset time. Images were analyzed by RadiAnt DICOM Viewer software (Medixant, Poznan, Poland) and ImageJ software (National Institutes of Health, USA). Slice thickness = 0.5 mm, TE = 22 ms, TR = 4500 ms.

The other methods were provided in Supporting information.

2.11. *Statistical analysis*

Statistics were performed as described in each Figure's captions. GraphPad Prism (version 9.0.0) was used for all statistical analyses. Values are presented as dot plots with individual data points plus bar, with mean ± SD, with $P < 0.05$ was considered statistically significant, unless otherwise noted. Unpaired Student's *t*-test or one-way or multi-way ANOVA followed by Tukey's multiple comparisons test as mentioned in the text were used for assessing the group differences.

3. Results

3.1. *ROS and PC induced hormesis effect of MSCs in stroke microenvironment*

In the infarct microenvironment after ischemic reperfusion injury, the ROS and PC play essential roles in the hormesis effect dependent on their levels. To explore the balance between beneficial and toxic levels for MSCs, we first tested the hormesis effects of MSCs based on conditioned mediums from proinflammatory cytokines-stimulated microglia. We prepared proinflammatory cocktails in gradient concentration consisting of three vital proinflammatory cytokines, TNF-α, IL-6, and IL-1β equivalently, and applied them to stimulate rat-derived HAPI microglia. Then, the conditioned mediums were collected to test MSC's vitality. An obvious hormesis phenomenon was observed (Fig. 1A), MSC vitality was improved in the conditioned mediums collected from 100 to 500 pg/mL proinflammatory cocktail stimulated HAPI microglia, then the vitality decreased along with the increase of proinflammatory cocktail level. We detected the TNF-α, IL-1β, IL-6, and H_2O_2 levels in conditioned mediums (Fig. 1B–E), finding the beneficial level for MSCs were 20–220 pg/mL (TNF-α), 13–130 pg/mL (IL-1β), 25–283 pg/mL (IL-6), 0.5–2 μmol/L (H_2O_2) respectively. To confirm the hormesis effects of MSCs, we further tested the MSC's vitality in cultured with different levels of TNF-α, IL-1β, IL-6, and H_2O_2 mediums. As shown in Fig. 1F–I, the beneficial dose levels for MSCs were 20–200 pg/mL (TNF-α), 20–100 pg/mL (IL-1β), 20–200 pg/mL (IL-6), 0.2–1 μmol/L (H_2O_2), respectively. Despite little differences, the beneficial dosage range matched the results of Fig. 1B–E. We further investigated the hormesis effects on MSC proliferation and mitochondrial homeostasis in high or low ROS and PC levels. It was shown in Fig. 1J that the MSCs proliferation was activated and improved in a low-level (0.5 μmol/L H_2O_2, 100 pg/mL proinflammatory cocktail), while inhibited in a high-level (10 μmol/L H_2O_2, 10 ng/mL proinflammatory cocktail). The low-level group was 2.6-fold than the high-level group in proliferation. Moreover, the mitochondrial membrane potential of MSCs in the high-level group decreased significantly resulting in the following apoptosis. In the low-level group, MSCs were as healthy as the normal were. All the results demonstrated that the strategy of utilizing the hormesis effect to enhance MSCs vitality would be effective and promising. As far as we protected MSCs from high toxic levels of ROS and PC, and established a livable niche with low beneficial levels of ROS and PC, the therapeutic efficiency of MSCs would be improved for their high vitality.

3.2. *HAPI microglia buffered high-level proinflammatory cytokines (PC)*

Microglia is the first responder in stroke brain injury *via* its sensitive interaction with PC[26]. Inspired by its unique role in stroke development, we assumed that the microglia had the potential to buffer excessive PC in the infarct microenvironment by the PC-receptors interaction. We selected rat-derived microglia cell line HAPI as the model microglia for research[37]. We found native HAPI was sensitive to PC stimulation at different levels (Fig. 2A). HAPI represented normal morphology below 100 pg/mL proinflammatory cocktails but atrophied and died more seriously along with the increase of PC level. The sensitive response between HAPI morphological changes and PC level was applied for the following PC buffer test. We designed a PC buffer assay to test the buffer effect of HAPI. As shown in Fig. 2B, the first PC (1 ng/mL)-contacting HAPI atrophied quickly in the buffer zone, while the secondary PC-contacting HAPI showed no obvious morphological changes. It's possibly for the reason that most of the high-level PC were absorbed and buffered by the first HAPI. The remaining PC were in low-level and left for the secondary HAPI. The phenomena inspired us that HAPI had great potential to be utilized as a PC-absorbing tool for modulating the hormesis effect in the infarct microenvironment. LPS-stimulated HAPI was reported to be more active in inflammatory development[38]. Hence, we tested the response of LPS-stimulated HAPI with a high-level PC (Fig. 2C). It's interesting to find that the LPS-stimulated HAPI showed better vitality and resistance against the high-level PC than the native HAPI. We explored the corresponding receptors on LPS-stimulated HAPI (Fig. 2D), and a higher expression level was observed in the LPS-stimulated HAPI group. After LPS-stimulated, IL-1R, IL-6R, TNFR1 and TNFR2 on HAPI were 1.45-, 1.46-, 2.05- and 2.6-fold higher than the native respectively. It revealed that the PC-receptors on HAPI were the key components involved in HAPI's PC-absorbing and buffer effect. To confirm this effect, we detected the PC level in a high-level proinflammatory cocktail containing medium, before (−1 min), and after (5 min, 10 min, 12 h, and 24 h) stimulation (Fig. 2E). The PC level decreased largely in 5- and 10-min points, indicating

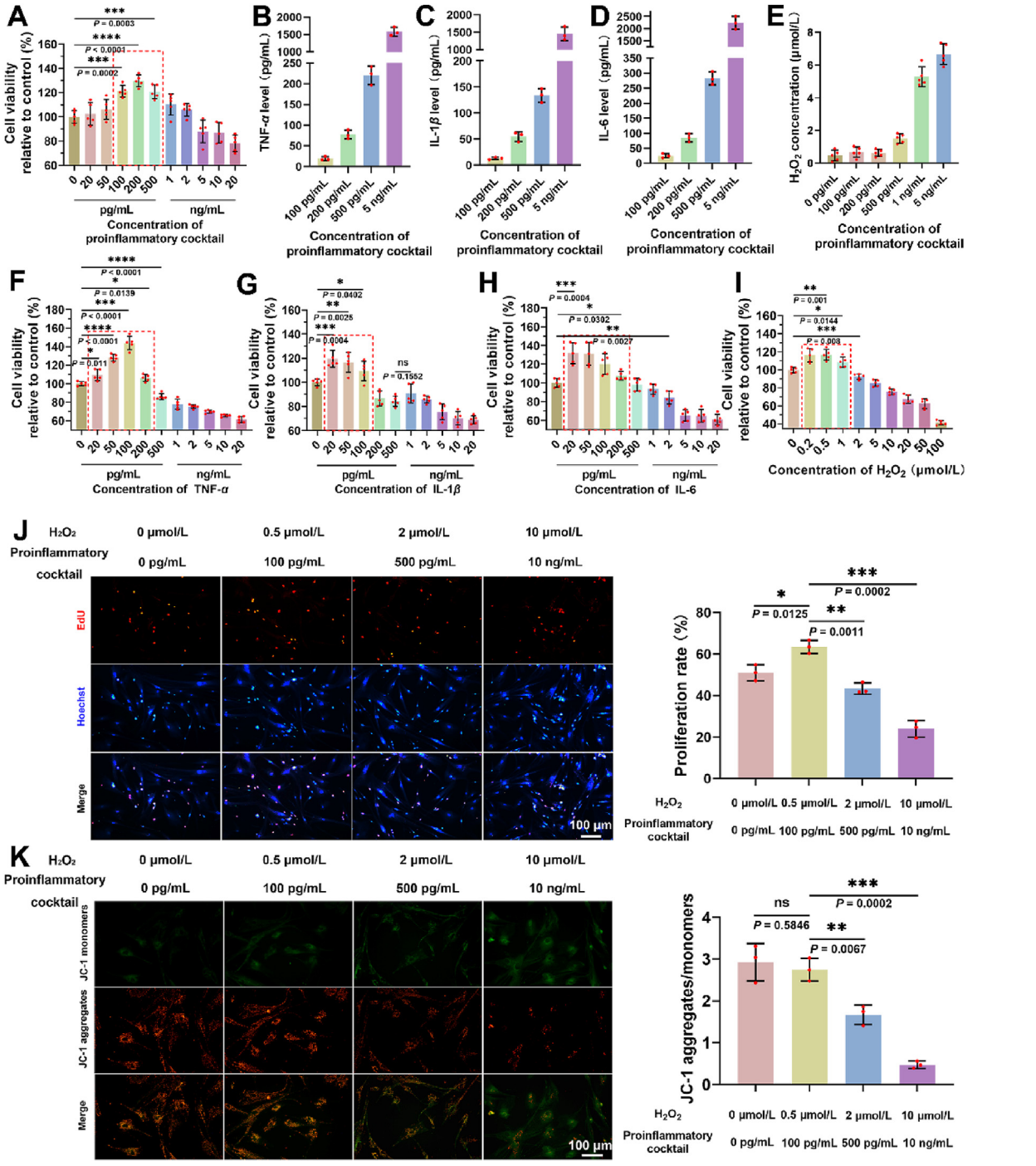

Figure 1 ROS and PC induced hormesis effect of MSCs in stroke microenvironment. (A) The MSC vitality after being cultured with different conditioned mediums from proinflammatory cocktail-stimulated HAPI microglia. $n = 5$. (B) The TNF-α level in conditioned mediums from proinflammatory cocktail-stimulated HAPI microglia. $n = 3$. (C) The IL-1β level in conditioned mediums from proinflammatory cocktail-stimulated HAPI microglia. $n = 3$. (D) The IL-6 level in conditioned mediums from proinflammatory cocktail-stimulated HAPI microglia. $n = 3$. (E) The H_2O_2 concentration in conditioned mediums from proinflammatory cocktail-stimulated HAPI microglia. $n = 5$. (F) The MSC vitality after being cultured with different TNF-α mediums. $n = 5$. (G) The MSC vitality after being cultured with different IL-1β mediums. $n = 5$. (H) The MSC vitality after being cultured with different IL-6 mediums. $n = 5$. (I) The MSC vitality after being cultured with different H_2O_2 mediums. (J) Proliferative activity of MSC after being cultured with different ROS and PC levels, detected by EdU assay. Representative images (Left), Quantitative analysis (Right), $n = 3$. Scale bar = 100 μm. (K) Mitochondrial membrane potential of MSC after being cultured with different ROS and PC levels, detected by JC-1 assay. Representative images (Left), Quantitative analysis (Right), $n = 3$. Scale bar = 100 μm. All data are shown as mean ± SD. $^*P < 0.05$, $^{**}P < 0.01$, $^{***}P < 0.001$ and $^{****}P < 0.0001$, one-way (A, F–K) ANOVA with Tukey's multiple comparisons test. ns, not significant.

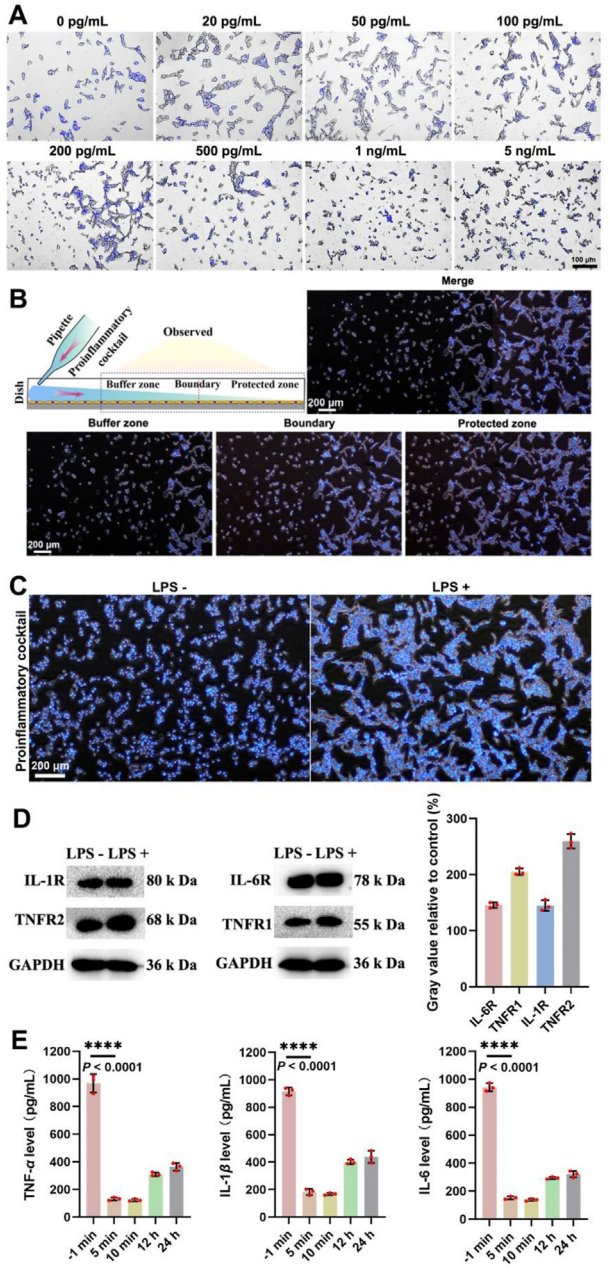

Figure 2 HAPI microglia buffered high-level proinflammatory cytokines (PC). (A) The morphological changes of HAPI microglia in gradient level proinflammatory cocktails. Bright-field observation merged with Hoechst labeled nucleus. Scale bar = 100 μm. (B) Proinflammatory cytokines buffer effect. The First PC (1 ng/mL)-contacting HAPI absorbed most of the PC in the buffer zone and protected the secondary PC-contacting HAPI in the protected zone. Darkfield observation merged with Hoechst labeled nucleus. Scale bar = 200 μm. (C). LPS-stimulated HAPI microglia show better PC buffer effects in morphology. Darkfield observation merged with Hoechst labeled nucleus. Scale bar = 200 μm. (D) Representative PC-absorbing receptors on HAPI (Left). Expression level relative to GAPDH (Right). $n = 3$. (E) TNF-α, IL-1β, and IL-6 levels in the proinflammatory cocktail, before (−1 min) or after (5 min, 10 min, 12 h, and 24 h) being absorbed by LPS-stimulated HAPI. $n = 3$. All data are shown as mean ± SD. ***$P < 0.001$ and ****$P < 0.0001$, one-way (E) ANOVA with Tukey's multiple comparisons test. ns, not significant.

a quick PC absorbing ability of LPS-stimulated HAPI. Then, when the absorbed PC converted to proinflammatory signals, 12 or 24 h after absorption, more PC were secreted, and this led to the increase of the PC level in the medium. Considering the PC-receptors were the main effective ingredients, we decided to extract the PC-receptors containing membrane from the LPS-stimulated HAPI to establish a PC buffer barrier for MSCs *via* biomimetic nanotechnology.

3.3. *Construction and characterization of the bioorthogonal microglia inspired MSC bioengineering system (LA-HM-NP-MSC)*

In preparation, metabolic glycoengineered MSCs were armed with LPS-stimulated HAPI microglia-derived membrane coating nanoparticles and an antioxidative protective layer (Fig. 3A). Firstly, we prepared the PLGA nanoparticles (NP) as frames to support the membrane (HM) coating *via* the emulsion solvent evaporation method[39–41]. Then a classical co-sonication was applied for membrane coating[42]. The amounts of PC-receptors on membrane coating NP directly affected its PC-absorbing efficiency. To achieve the optimized membrane coating ratio, we explored the properties of HM-NP corresponding to the weight ratio of membrane to PLGA. The protein content of HM-NP was positively correlated to the weight ratio but was close to saturation when the ratio exceeded 1.0 (Fig. 3B). Meanwhile, the size and zeta potential were both close to the maximum, when the ratio reached 1.0 (Fig. 3C and D). Membrane coating increased the size by approximately 25 nm and decreased the zeta potential by approximately 22.8 mV. These results characterized the successful preparation of HM-NP and revealed that 1.0 (weight ratio of membrane/PLGA) was the optimized membrane coating ratio. Thus, we prepared the HM-NP in this ratio and its average size was 109.8 nm, zeta potential was −19 mV. Then, we tested the PC-absorbing capacity of HM coating nanoparticles. As represented in Fig. 3E−G, LA-HM-NP, and HM-NP both showed a similar absorbing trend with the vehicle and decreased the PC level significantly with the increase of nanoparticle's concentration. The remaining TNF-α, IL-1β, and IL-6 in the LA-HM-NP group were only 6.7%, 18.5%, and 8.3% of the NP group. These results proved that the PC-absorbing capacity was well retained after the preparation process, and the LA anti-oxidative layer decoration would not affect the PC-absorbing capacity.

To arm the MSCs with HM-NP in the physiological microenvironment, a bioorthogonal reaction between dibenzylcyclooctyne (DBCO) and azide (N_3) was introduced[20]. Ac4GalNAz was used for modifying MSC to get the MSC-N_3 *via* metabolic glycoengineering. DBCO-PEG-DSPE was chosen as the linker between HM-NP and MSC-N_3 to establish this system. For confirming the bioorthogonal connection of DBCO-HM-NP and MSC-N_3, fluorescent indicator coumarin-6 was loaded in NP for detection. As represented in Fig. 3H, the natural uptake group (NP + MSC) showed high fluorescence intensity. After HM coating, HM-NP and PEG-HM-NP decreased the uptake amount, possibly due to the evasion effect of HM and the hydration shell of PEG[43]. However, with the insertion of DBCO-PEG-DSPE, the DBCO-HM-NP-MSC group exhibited 6.6-fold higher fluorescence intensity than the PEG-HM-NP + MSC group. It demonstrated that more DBCO-HM-NPs were labeled on MSCs, more possibly due to the bioorthogonal reaction between DBCO and N_3-. For visualizing the bioorthogonal decoration of DBCO-HM-NP and LA-PEG-N_3 in this system, coumarin-6 was loaded to visualize NP and sulfo-Cy3-N_3 was used as LA-PEG-N_3's simulant. In

fluorescence imaging (Fig. 3I), DBCO-HM-NPs distributed on the surface of MSCs unevenly. Sulfo-Cy3-N_3 showed colocalization with DBCO-HM-NPs, while PEG-HM-NPs were distributed in the cytoplasm evenly. What's more, in Fig. 3J and Supporting information Fig. S1, scanning electron microscope (SEM) images showed that large amounts of white nano-dots were distributed on LA-HM-NP-MSC's surface. While there were no evident white nano-dots on the surface of MSC. Considering the recording principle of SEM, only the NPs binding on the cellular surface could be recorded in SEM images, endocytosed NPs could not be observed on the cellular surface. We inferred that the white spots were binding DBCO-HM-NPs and tended to confirm that most of the DBCO-HM-NPs were bioorthogonally bound on the surface of MSC.

3.4. *LA-HM-NP-MSC buffered high-level ROS and PC to improve MSC vitality*

The "cellular surface arming" engineering could endow MSCs with great ROS scavenging and PC-absorbing capacity, while not exerting any negative effects on MSCs' differentiation potential (Supporting information Fig. S2). Here, we evaluated the ROS and PC buffer effects of LA-HM-NP-MSC *in vitro*. In the H_2O_2 scavenging assay (Fig. 4A), the LA-HM-NP-MSC group's H_2O_2 level decreased to 44.8 μmol/L in 15 min and 23.5 μmol/L in 30 min, but the MSC group's H_2O_2 level only decreased to 80 μmol/L in 15 min and 54.3 μmol/L in 30 min. LA antioxidative protective layer exerted a highly efficient reactive oxygen species elimination and protected MSC from high toxic level ROS, increasing 2.34-fold MSC vitality (Fig. 4B). In addition to the quick ROS scavenging effect, LA-HM-NP-MSC also exhibited stronger PC-absorbing capacity than native MSC. It showed that the PC-absorbing capacity was in positive correlation with the number of cells. When the LA-HM-NP-MSC numbers increased to 1×10^6, the left PC in the absorbing solutions was only 16.8% (TNF-α), 9.8% (IL-1 β), 21.3% (IL-6) of the MSC group respectively (Fig. 4C). They decreased to 179.7 ± 16.1 pg/mL (TNF-α), 84.3 ± 10.84 pg/mL (IL-1 β), and 65.9 ± 1.6 pg/mL (IL-6), were all in coincidence with the beneficial dose level for MSCs (Supporting information Figs. S3 and S4). What's more, in Fig. 4D, the HAPI in the buffer zone didn't atrophy in morphology, indicating a low-level PC was achieved after the absorption. Meanwhile, the cell growth morphology evaluation in Supporting information Fig. S5 also showed that LA-HM-NP-MSCs could maintain a healthy cell growth morphology under 10 ng/mL PC injury, while the native MSC appeared to atrophy. These results confirmed that high-level PC could be buffered to the low-level by LA-HM-NP-MSC and effectively protected MSC from high-level PC injury. These results above not only proved the successful "cellular surface arming" engineering, but also proved the potential capacity of LA-HM-NP-MSC to remodel the infarct microenvironment, modulate the hormesis effect, and create livable micro-niche for MSCs *in vivo*.

Then, we further evaluated the protection and vitality-enhanced effects of LA-HM-NP-MSC. In a high-level ROS and PC microenvironment, LA-HM-NP-MSC barely got oxidative stress injury but native MSC was significantly damaged. In the oxidative stress assay, the LA-HM-NP-MSC group showed a low intracellular ROS level, which was only 32.7% of the MSC group, indicating the great anti-oxidative stress effect of this system (Fig. 4E). Meanwhile, the mitochondrial membrane potential of LA-HM-NP-MSC was in a healthier state, 5.2-fold more stable than MSC (Fig. 4F and G). What's more, the proliferation activity of LA-HM-NP-MSC was enhanced, showing 2.6-fold higher than MSC in the high-level ROS and PC microenvironment (Fig. 4H and I). It's possibly for the hormesis effect, that high toxic level ROS and PC were buffered to low beneficial levels by the extracellular PC absorption and ROS scavenging. The surface arming constructed a livable micro-niche for MSCs to enhance their biological activity.

Then, the importance between PC absorbing and ROS scavenging effects on MSCs was compared in Supporting information Fig. S6. As shown in Fig. S6A, cell viability of different surface arming MSC under 10 ng/mL PC and 10 μmol/L H_2O_2 was detected. The MSC viability of LA-NP-MSC was higher than HM-NP-MSC, while LA-HM-NP-MSC was higher than both of them. Besides, in Fig. S6B, the NIRF signals of intravenously transplanted MSCs with different surface arming in *ex vivo* brains on Day 7, the intensity of LA-HM-NP-MSC was 1.4- and 4.2-fold stronger than the LA-NP-MSC group and HM-NP-MSC group respectively, while LA-NP-MSC was 2.9-fold stronger than HM-NP-MSC. These results demonstrated that the ROS scavenging effect was more important than the PC absorbing effect in protecting MSC viability, possibly due to the direct oxidative injury being more severe than the indirect injury of PC. While, the PC buffer effect could then exert a better vitality-enhanced effect on MSC *via* the hormesis effect, after surviving from oxidative killing. In summary, decreasing both PC and ROS showed a better beneficial effect than only decreasing one of them. Additionally, we tested the long-term ROS scavenging and PC absorbing ability of LA-HM-NP-MSC in the medium containing 15% fetal bovine serum (FBS). As shown in Supporting information Fig. S7, both the ROS scavenging and PC absorbing ability could be maintained above 80% 48 h after preparation. What's more, the ROS and PC levels were higher in the infarct microenvironment in the first 48 h, thus the stability of LA-HM-NP-MSC would be efficient for protecting MSC and enhancing the therapeutic efficiency after injection.

3.5. *LA-HM-NP-MSC achieved enhanced engraftment efficiency as well as cognitive and motor functional recovery*

In this system, the transplanted MSC vitality in the infarct brain was closely related to the surface arming degree. Different arming degree would affect the protection and buffer effect of LA-HM-NP-MSC. Thus, we prepared LA-HM-NP-MSCs with different surface arming degree by adjusting the weight ratio of the HAPI membrane to PLGA. MSC group (0%) was native MSC without any modification, the 20% group was prepared in 0.2 weight ratio, the 50% group was prepared in 0.5 weight ratio, 100% group was prepared in 1.0 weight ratio. After preparation, the ROS scavenging and PC-absorbing capacity of MSCs with different surface arming degree were tested *in vitro* (Supporting information Fig. S8). The 100% LA-HM-NP-MSC showed the best ROS scavenging and PC-absorbing capacity, while the 50%, 20%, and MSC (0%) were in gradual decline.

Then, we evaluated the *in vivo* vitality-enhanced efficiency of MSCs with different surface arming degree by a near-infrared fluorescence (NIRF) MSC tracking method. A transient middle cerebral artery occlusion (MCAO) model was made for the following research[44]. In brief, a NIRF dye DIR was loaded into NP, and labeling MSC in a bioorthogonal route. As represented in Fig. 5A and B, the NIRF signal of the 100% group kept increasing from the 1st day to the 7th day. On Day 1 after transplantation, the intensity of the 100% group was 2.9-fold than that of the MSC group, while on Day 7, the intensity increased to 5.5-fold. The

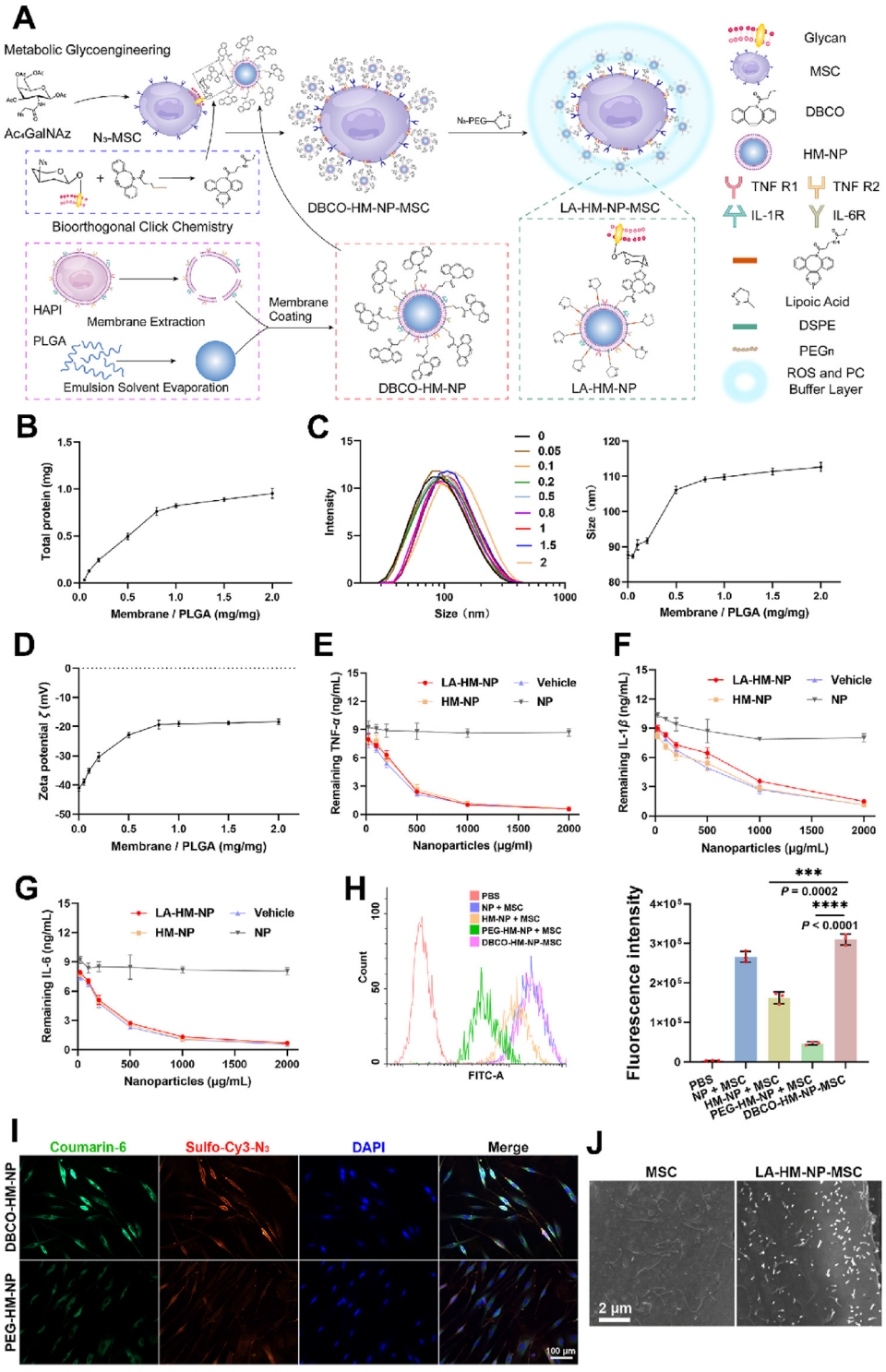

Figure 3 Construction and characterization of the bioorthogonal microglia inspired MSC bioengineering system (LA-HM-NP-MSC). (A) Illustration of preparing LA-HM-NP-MSC. Metabolically glycoengineering MSCs to translate-N_3 in the MSC surface's glycan (N_3-MSCs). Then N_3-MSCs were armed with DBCO-PEG-DSPE anchored HAPI membrane coating nanoparticles (DBCO-HM-NP) bioorthogonally to get the DBCO-HM-NP-MSC, which could buffer the high-level PC. Finally, lipoic acid-PEG-N_3 armed on the surface of the DBCO-HM-NP-MSC (LA-HM-NP-MSC) bioorthogonally to establish an extracellular antioxidative layer, which could efficiently protect intravenously transplanted MSCs from ROS injury. (B) Protein content of different membrane/PLGA weight ratios. $n = 3$. (C) Hydrodynamic size distribution of different membrane/PLGA weight ratios (Left). The relationship of size and membrane/PLGA weight ratio (Right). $n = 3$. (D) The relationship of zeta potential and membrane protein/PLGA ratio. $n = 3$. (E) TNF-α-absorbing property of LA-HM-NP. $n = 3$. (F) IL-1β-absorbing property of LA-HM-NP. $n = 3$. (G) IL-6-absorbing property of LA-HM-NP. $n = 3$. (H) Mean fluorescence intensity of different formulations' MSCs labeling measured by flow cytometry. $n = 3$. Fluorescence probe Coumarin-6 loaded in NP as an indicator. PBS as the negative control. (I) Visualization of

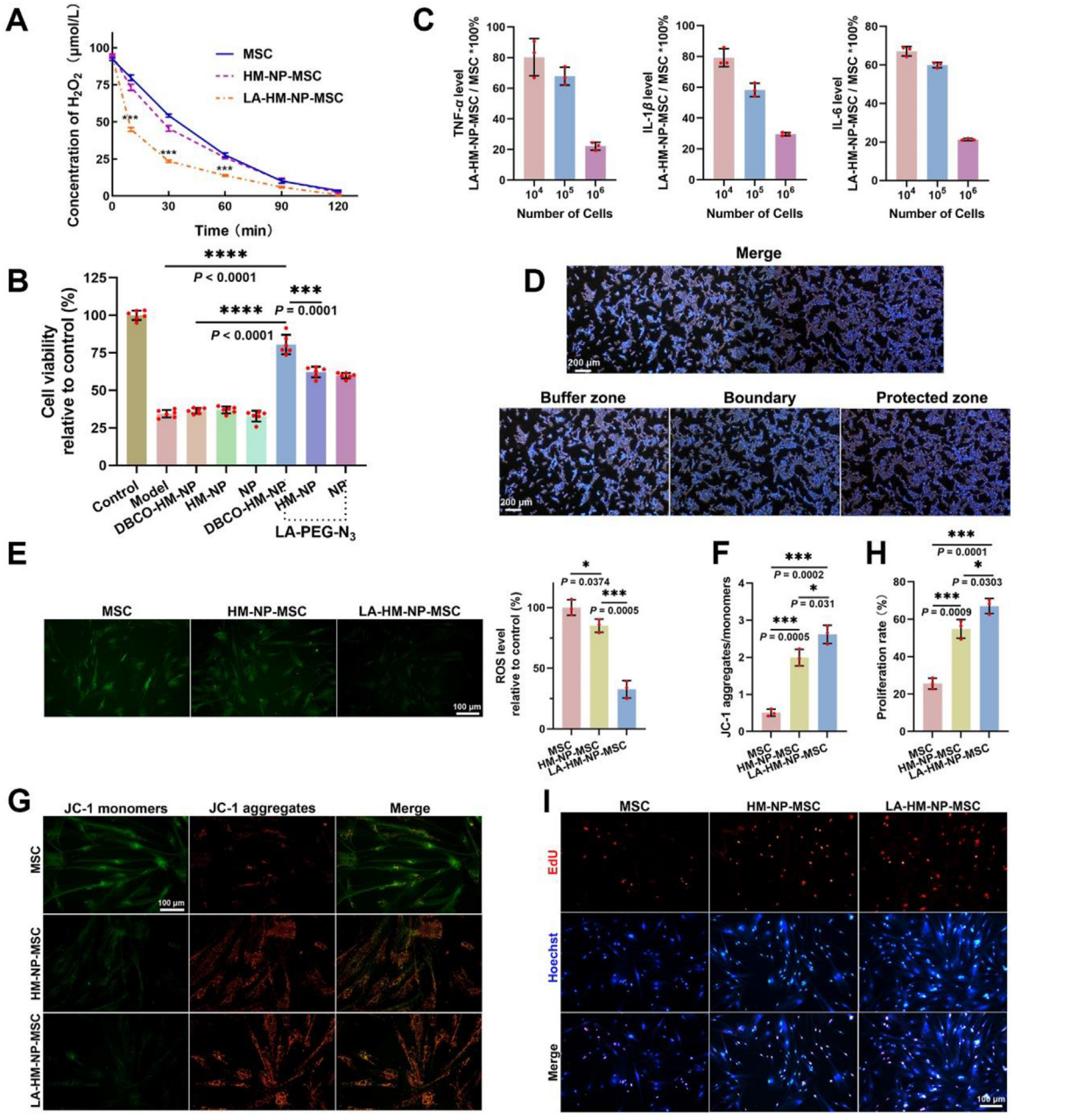

Figure 4 LA-HM-NP-MSC buffered high-level ROS and PC to improve MSC vitality. (A) ROS scavenging capacity of LA-HM-NP-MSC. $n = 3$. (B) MSC viability after 100 μmol/L H_2O_2 erosion. $n = 6$. (C) PC-absorbing capacity of LA-HM-NP-MSC, relative to native MSC. $n = 3$. (D) PC buffer assay tested the PC level after being co-cultured with LA-HM-NP-MSC. Primary PC level = 10 ng/mL, scale bar = 200 μm. (E) Intracellular ROS detected by DCFH-DA. Representative images (Left), scale bar = 200 μm. Quantitative analysis (Right), $n = 3$. (F) Quantitative analysis of mitochondrial membrane potential. $n = 3$. (G) Representative images of mitochondrial membrane potential after 10 ng/mL PC and 100 μmol/L H_2O_2 erosion, detected by JC-1 assay, scale bar = 100 μm. (H) Quantitative analysis of proliferation. $n = 3$. (I) Representative images of proliferation after 10 ng/mL PC and 100 μmol/L H_2O_2 erosion, tested by an EdU assay, scale bar = 100 μm. All data are shown as mean ± SD. $^*P < 0.05$, $^{***}P < 0.001$, and $^{****}P < 0.0001$, one-way (B, E, F, H) or multi-way (A) ANOVA with Tukey's multiple comparisons tests. ns, not significant.

20% and 50% group also showed improvements to some extent according to their surface arming degree. On Day 7, the *ex vivo* NIRF signal evidenced the results above as well (Fig. 5C and D). The intensity of the 100% group was 5.1-fold than the MSC group, while 50% and 20% were 2.9- and 1.9-fold than the MSC group respectively. It indicated that LA-HM-NP-MSC could achieve higher engraftment in the infarct area with the increase of surface arming degree. These *in vivo* or *ex vivo* NIRF results

bioorthogonal decoration among N_3-MSC, DBCO-NP, and LA-PEG-N_3 in fluorescence (sulfo-Cy3-N_3 was chosen as LA-PEG-N_3's simulant), scale bar = 100 μm. (J) Representative SEM images, scale bar = 2 μm. All data are shown as mean ± SD. $^{***}P < 0.001$ and $^{****}P < 0.0001$, one-way (H) ANOVA with Tukey's multiple comparisons test. ns, not significant.

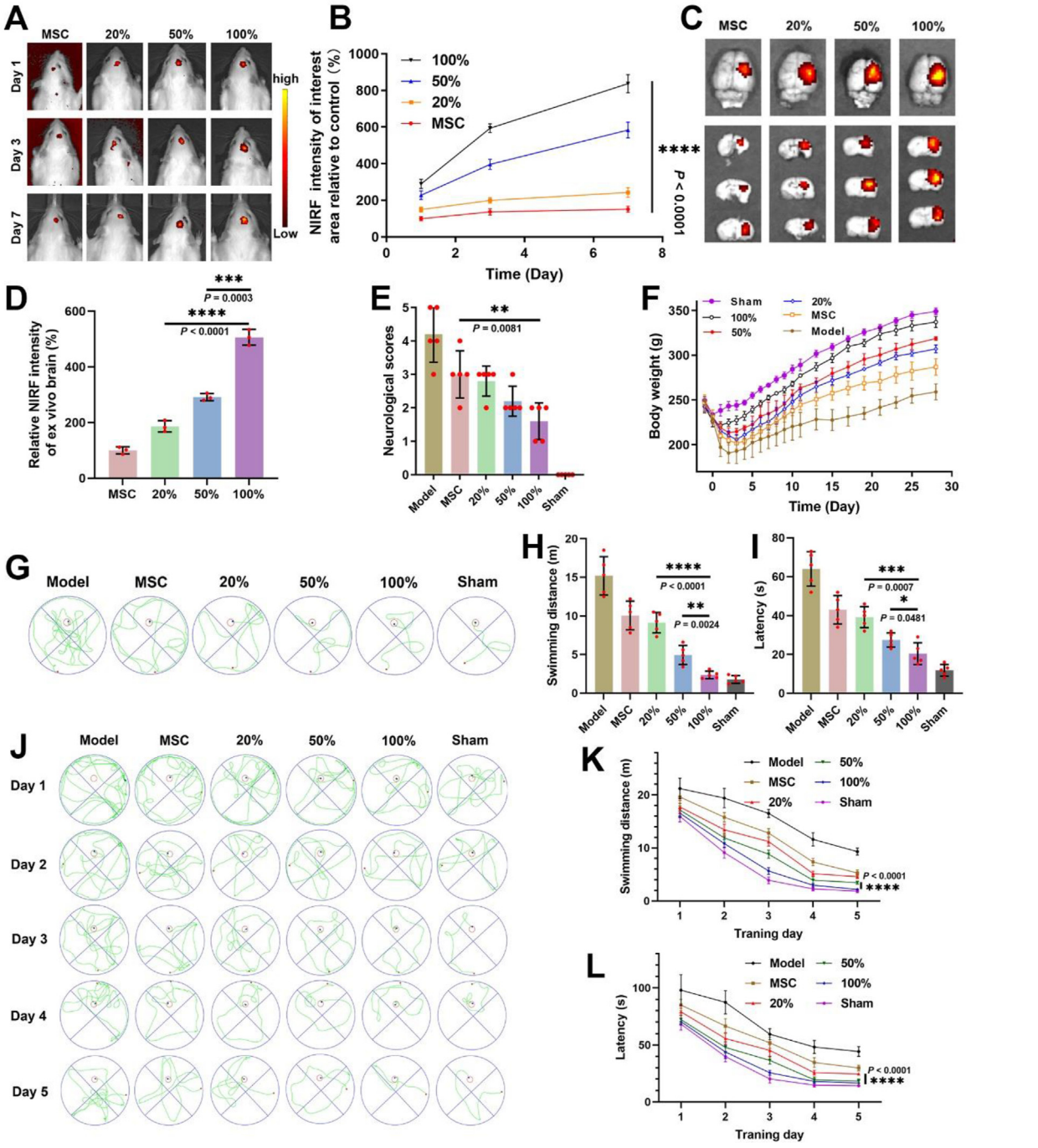

Figure 5 LA-HM-NP-MSC achieved enhanced engraftment efficiency as well as cognitive and motor functional recovery. (A) *In vivo* NIRF tracking after intravenously transplanted MSCs with different surface arming degree. (B) The curve of the NIRF signal changes *in vivo*. $n = 5$. (C) NIRF signals of intravenously transplanted MSCs with different surface arming degree in *ex vivo* brains on Day 7. (D) Qualification of NIRF intensity in *ex vivo* brain on Day 7. $n = 3$. (E) Neurological score evaluation on Day 3 after MSC treatment, $n = 5$. (F) Health-related body weight recorded from 1 day before the surgery to 28 days after MSC treatment, $n = 5$. (G) Morris water maze assays on tested rats 3 days after MSC treatment. (H) Swimming distance analysis of tested rats 3 days after MSC treatment. $n = 5$. (I) Latency analysis of tested rats 3 days after MSC treatment. $n = 5$. (J) Morris water maze assays on tested rats 28 days after MSC treatment. (K) Swimming distance analysis of tested rats 28 days after MSC treatment. $n = 5$. (L) Latency analysis of tested rats 28 days after MSC treatment. $n = 5$. All data are shown as mean ± SD. $^*P < 0.05$, $^{**}P < 0.01$, $^{***}P < 0.001$ and $^{****}P < 0.0001$, one-way (B, D, E, H, I, K, L) ANOVA with Tukey's multiple comparisons test. ns, not significant.

demonstrated that native transplanted MSCs in the infarct microenvironment suffered from the threats of high-level ROS and PC, and could not achieve a high engraftment in the infarct brain. In contrast, the bioengineered LA-HM-NP-MSC maintained a high vitality and engraftment in the infarct area with the ROS and PC dual-buffer barrier. The surface arming strategy could protect

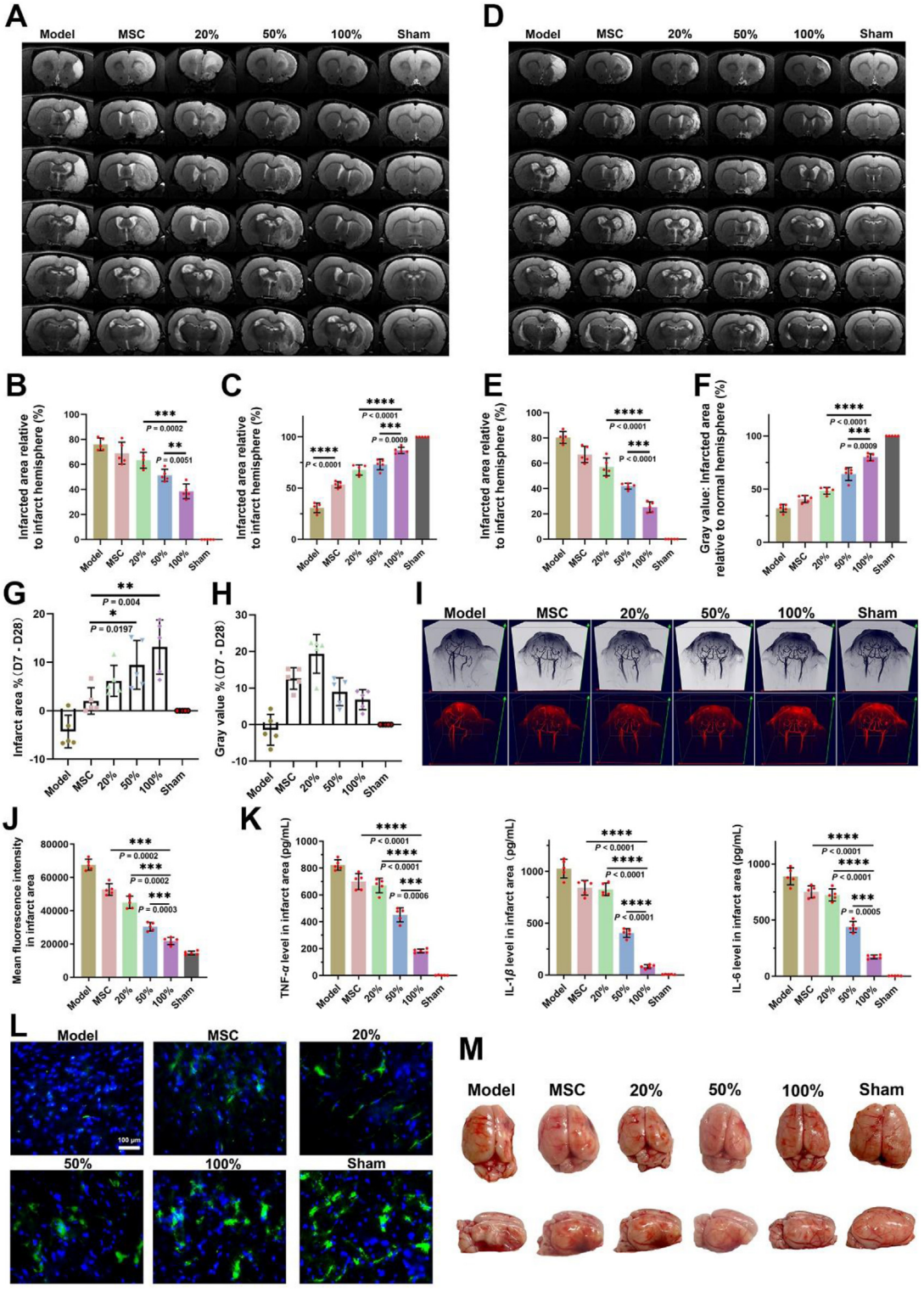

Figure 6 The mechanism of LA-HM-NP-MSC's enhanced anti-stroke therapeutic effects. (A) T_2 MRI of the stroke rats 7 days after MSC therapy. (B) Infarct area of the stroke rats 7 days after MSC therapy. $n = 5$ (C) Gray value of infarct area of T_2 MRI 7 days after MSC therapy. $n = 5$. (D) T_2 MRI of the stroke rats 28 days after MSC therapy. (E) Infarct area of the stroke rats 28 days after MSC therapy. $n = 5$ (F) Gray value of infarct area of T_2 MRI 28 days after MSC therapy. $n = 5$. (G) Infarct area changes between the values of Day 7 and Day 28. $n = 5$. (H) Gray value changes between Day 7 and Day 28. $n = 5$. (I) Vascular MRI of the cerebral vessels 28 days after MSC therapy. (J) ROS level in infarcted area 3 days after MSC therapy. $n = 5$. (K) Proinflammatory cytokines in infarcted area 3 days after MSC therapy. TNF-α level (Left), IL-1β level (middle), IL-6 level (Right). $n = 5$. (L) Representative NeuN immunofluorescence images in infarcted area 2 months after MSC treatment, scale bar = 100 μm. (M) Representative images of brain volume loss 2 months after MSC therapy. All data are shown as mean ± SD. $^*P < 0.05$, $^{**}P < 0.01$, $^{***}P < 0.001$, and $^{****}P < 0.0001$, one-way (B, C, E, F, G, H, J, K) ANOVA with Tukey's multiple comparisons test. ns, not significant.

and enhance MSC vitality effectively by creating a livable microniche for transplanted MSCs. Moreover, the vitality-enhanced effects of LA-HM-NP-MSC were closely related to the surface arming degree.

With the improvement of MSC engraftment and vitality, the anti-stroke effects of LA-HM-NP-MSC in stroke acute and subacute phase were explored. Firstly, neurological scores were assessed three days after injection. Results showed that the 100% group obtained 1.6 points compared with 3 points of the MSC (0%) group (Fig. 5E). Meanwhile, we monitored the survival rates and health-related body weight of the tested rats in different groups. The model group's body weight decreased by 15.6% during the acute phase (Day 3), however, the 100% group showed no significant difference (Fig. 5F). Moreover, the 100% group exhibited the quickest recovery and increase in body weight during the sub-acute phase (Days 3−28). The survival curve showed that the 100% group got 80% survival while the MSC group was only 53% on Day 3 (Supporting information Fig. S9). Besides, there were no more deaths in the sub-acute phase of the 100% group, indicating a sustained protection effect on stroke rats. To evaluate the therapeutic effects on cognitive and motor function, the Morris water maze was performed after MSC therapy[45]. Firstly, we tested the trained rats (training for 5 days before stroke) of different groups on Day 3 (Fig. 5G). Swimming paths showed that the 100% group arrived at the target platform in the shortest path and spent the least time than the MSC (0%) group (Fig. 5H and I). It exhibited that LA-HM-NP-MSC exerted significant neuroprotection effects on stroke rats in the acute phase. After recovery for 28 days, we continued to evaluate the neurological function of the Morris water maze (Fig. 5J). During the training process, the 100% group showed a better learning and motor ability that was nearly the same as the sham group, while the MSC (0%) group was only slightly better than the model group (Fig. 5K and L). It suggested that the 100% surface armed MSCs had better and sustained therapeutic effects probably due to the higher MSC vitality. In all, the results above revealed that LA-HM-NP-MSC could inhibit acute Ischemic reperfusion injury after stroke effectively, and its therapeutic effects would get better and last longer with the surface arming degree increased.

3.6. The mechanism of LA-HM-NP-MSC's enhanced anti-stroke therapeutic effects

Surface arming endowed MSC with stronger infarct microenvironment remodeling capacity, and showed better therapeutic effects on stroke rats than native MSC both in acute and sub-acute phase. Here, we explored the mechanism of LA-HM-NP-MSC's enhanced anti-stroke therapeutic effects. T_2 MRI is a commonly used clinical diagnostic technique for stroke, which can reflect the infarct area and severity in precise[46]. On Day 7 after MSC therapy, it was observed that severe infarct area appeared in all stroke groups, but the severity was significantly different (Fig. 6A). With the increase of surface arming degree, the relative infarct area decreased slightly from 69% (MSC group) to 39% (100% group) (Fig. 6B). What's more, the relative gray value (severity) in the infarct area was the key indicator reflecting the protection and therapeutic effects, that lower value indicated the infarcted injury was worse and the therapeutic effects were insufficient. The MSC (0%) group showed significant positive effects on stroke rats that increased the relative gray value from 30% (Model group) to 53% (MSC group) (Fig. 6C). With the increase in surface arming degree, the 100% group achieved a better result (87%). These phenomena demonstrated that the MSC therapy was effective in the early phase of stroke treatment, and the surface arming on MSC could improve the protection and therapeutic effects. However, when the pathological process developed to the later phase (Day 28 after MSC therapy), the T_2 MRI outcomes of different LA-HM-NP-MSC groups were greatly different from the outcomes of Day 7 (Fig. 6D−F). In general (Fig. 6G and H), the untreated stroke rats were even more serious in the aspect of infarct area and severity, while the MSC-treated groups (including MSC, 20%, 50%, and 100% groups) all showed decreased infarcted area and increased relative gray value (severity). It indicated that deterioration happened during the sub-acute phase of pathological development. However, with the increase of surface arming degree ($\geq$50%), the deterioration was effectively alleviated. A better cerebral vessel repair was achieved in high surface arming degree groups (Fig. 6I). We supposed it was the hormesis effect that contributed to these results. In harsh infarct area, high-level ROS and PC were detrimental to transplanted MSCs and inhibited the therapeutic effects on infarct brain. Low surface arming degree groups (MSC and 20% group) couldn't scavenge the high-level ROS and PC in the infarct microenvironment effectively (Fig. 6J and K), leading to low engraftment and vitality of transplanted MSCs. The ROS level in the infarct area of the 100% group decreased by 58.6% than the MSC group. The PC levels in the infarct microenvironment were only 23.3% (TNF-α), 7.9% (IL-1β), and 20.3% (IL-6) of the MSC group, decreased to 182.8 $\pm$ 14 pg/mL, 81.2 $\pm$ 18.3 pg/mL and 172.2 $\pm$ 16.4 pg/mL respectively, which were all in coincidence with the beneficial dose level for MSCs. Despite positive therapeutic effects observed in the early phase, the serious deterioration was not inhibited. On the contrary, high surface arming degree groups (50% and 100% group) not only remodeled the harsh microenvironment, but buffered ROS and PC from the toxic high-level to the beneficial low-level, constructing a livable niche for transplanted MSCs in infarct area as well. On the one hand, highly armed LA-HM-NP-MSC exerted neuroprotective effects on the infarcted area (Fig. 6L and Supporting information Fig. S10) by scavenging excessive ROS and PC. On the other hand, the high toxic level ROS and PC were buffered to low beneficial level that enhanced MSC vitality and bioactivity and finally exerted a long-term therapeutic outcome. In the brain's morphology evaluation, the encephalatrophy of the 100% group was significantly inhibited compared with the Model group 2-month after MSC treatment (Fig. 6M). Meanwhile, both the MSC (0%) group and the 20% group showed obvious defects in the infarct area. In brain volume analysis, the 100% group exhibited 9.8 $\pm$ 5.6% volume loss compared to the 43.3 $\pm$ 6.8% of the Model group (Supporting information Fig. S11).

In total, the enhanced anti-stroke therapeutic effects mechanism of LA-HM-NP-MSCs is that a high surface arming degree of LA-HM-NP-MSC could efficiently scavenge and convert high-level ROS and PC, decrease the toxic effects and increase MSC vitality for therapeutic efficiency. However, the low surface arming degree of LA-HM-NP-MSC was insufficient to remodel the harsh microenvironment and modulate hormesis effects for its limited ability of ROS and PC scavenging, resulting in low MSC vitality and bad therapeutic effects.

4. Discussion

MSC provided great potential for stroke treatment in reversing the high lethality and morbidity. Compared with intracranial transplantation, the intravenous injection of transplanted MSCs shows better safety and patient compliance for its non-invasion and

convenience. However, the unstable therapeutic mechanism and results caused by their fragile viability are more serious and still the main challenges that keep hindering the clinical application of intravenous MSC therapy in stroke treatment. Great different from conventional drug therapy, MSCs are living and dynamic cells, that are extremely sensitive to microenvironmental changes including the surrounding extracellular matrix, signal factors, and ROS. These microenvironmental changes are usually double-sword in MSCs' bioactivity and vitality, such as high-level ROS and PC hurt MSCs, but low-level ROS and PC active MSCs. This hormesis effect increases the pathological complexity and poses a great threat to traditional stroke treatment, but brings the dawn for MSC therapy with artificial engineering.

In MSC artificial engineering, cytokine expression-enhanced genetic engineering and hypoxia preconditioning are common methods to augment anti-stroke efficiency in research[47,48]. Based on these methods above, MSCs have the potential to achieve better inflammation regulation and regeneration promotion but also face higher tumorigenicity. However, these methods hardly protect MSCs from the overproduced and excessive accumulated ROS and PC in the infarct microenvironment upon the transplanted MSCs arrive in the infarct area. Thus, it's essential for MSCs to be armed with a protective and activity-enhanced umbrella, without high tumorigenicity, to resolve this challenge. Previous studies have exhibited many ROS scavenging strategies to eliminate excessive ROS in infarct core, such as developing antioxidative drug, nano-enzyme, or their combinations[49], but few researches reported effective PC scavenging methods in infarct brains. Moreover, existing MSC protection or microenvironment remodeling strategies could only address the crisis of the high toxic ROS and PC level, but exert no effects on enhancing MSC vitality. In this study, a biomimetic "cellular surface arming" strategy without genetic engineering was first proposed. This strategy could not only handle the crisis of high toxic ROS and PC level, protect transplanted MSC in infarct harsh microenvironment simultaneously, but also modulate the hormesis effect to improve bioactivity and vitality of MSC, enhance the anti-stroke efficacy.

Inspired by the inflammatory modulator role of microglia *via* PC-receptor mode in ischemic stroke, we constructed a ROS and PC dual-buffer barrier over MSC *via* biomimetic nanotechnology and bioorthogonal engineering. PC-absorbing HAPI membrane coating nanoparticles and LA antioxidative agent were armed on metabolic glycoengineered MSC's surface in a mode of modular assembly. The ROS and PC dual-buffer barrier could exert two key functions and create livable niches in MSC therapy to treat stroke. Firstly, at the tissue level, the surface arming could scavenge both high-level ROS and PC, then remodel the infarct microenvironment to create a livable niche for injured neurons. Secondly, at a single MSC level, the surface arming could buffer the ROS and PC from high-level toxic effects to low-level beneficial effects, then create a micro-livable niche for MSC to activate and improve MSC bioactivity. Benefiting from the livable niches established by this biomimetic surface arming system, the MSC vitality was improved up to 5-fold, and therapeutic results of MSCs were promoted in efficiency and sustainability significantly.

Mentioning the limitations of this study, an in-depth mechanism of the hormesis effect on MSC was lacking. Although hormetic regions of these factors TNF-α, IL-1β, IL-6, and ROS were investigated, more contributing factors were involved in this process in the stroke microenvironment. The relationship among these factors was worth further study. What's more, this study proposed the idea of "cellular surface arming" for cell therapy and established a new non-genetic cellular engineering platform. There is still huge improvement in biomaterials selection, anti-oxidative enhancement, and proinflammatory cytokines buffer method to protect and strengthen MSC bioactivity cooperatively. As for the proinflammatory cytokines buffer method, the immune cell membrane materials seemed to be the preferred effective tool in neutralizing the excessive cytokines. However, the problems of source and potential immunological reaction possibly hinder the clinical translation of immune cell membrane materials. Therefore, developing alternative cell membrane biomimetic functional materials would promote clinical translation.

5. Conclusions

In general, we built a microglia-inspired MSC bioengineering system to strengthen MSC therapy for stroke, based on the intrinsic hormesis effects in cellular biology. In this system, extracellular ROS-scavenging and PC-absorbing layers could effectively scavenge the overproduced ROS and PC in infarct brain, and convert their deleterious effects to beneficial vitality enhancers for transplanted MSCs and injured neurons. Finally, better therapeutic improvements were achieved in both acute phase and chronic phase after MSC therapy. This vitality-augmented system demonstrates the potential to accelerate the clinical translation of MSC treatment and boost stroke recovery.

Acknowledgments

This work was supported by National Natural Science Foundation of China (Nos. 92068110, 81973272 and 92068111), Shanghai Science and Technology Committee (Nos. 20JC1411800, and 23S41900100, China), Programs of Shanghai Academic/Technology Research Leader (Nos. 21XD1400200 and 21XD1422200, China), Innovation Program of Shanghai Municipal Education Commission (2023ZKZD21, China), the fund of Research Grant for Health Science and Technology of Shanghai Municipal Commission of Health Committee (No. 20214Y0268, China), Science and Technology Development Fund of Shanghai Pudong New Area (No. PKJ2020-Y49, China) and the Project of Key Medical Specialty and Treatment Center of Pudong Hospital of Fudan University (No. Zdzk2020-15, China). We thank the Core Facility of Basic Medical Sciences, Shanghai Jiao Tong University School of Medicine, for technical and instrument assistance.

Author contributions

Jianpei Xu, Jun Chen, Xiaoling Gao designed the experiments. Jianpei Xu, Jun Chen, You Yang, Yuwen Zhang, Dan Huang, Songlei Zhou, Yipu Liu, Shiqiang Tong, Fenfen Ma, Qingxiang Song, Chengxiang Dai, Suke Li, Jigang Lei, and Zhihua Wang. performed the experiments and collected the data. All authors contributed to writing the manuscript, discussing the results and implications, and editing the manuscript at all stages. All of the authors have read and approved the final manuscript.

Conflicts of interest

The authors declare no competing financial interest.

Appendix A. Supporting information

Supporting data to this article can be found online at https://doi.org/10.1016/j.apsb.2023.11.009.

References

1. Li JS, Zhang Q, Wang W, Lin F, Wang S, Zhao JZ. Mesenchymal stem cell therapy for ischemic stroke: a look into treatment mechanism and therapeutic potential. *J Neurol* 2021;**268**:4095−107.
2. Kawabori M, Shichinohe H, Kuroda S, Houkin K. Clinical trials of stem cell therapy for cerebral ischemic stroke. *Int J Mol Sci* 2020;**21**:7380.
3. Chari S, Nguyen A, Saxe J. Stem cells in the clinic. *Cell Stem Cell* 2018;**22**:781−2.
4. You Y, Xu JP, Liu YP, Li HC, Xie LZ, Ma CC, et al. Tailored apoptotic vesicle delivery platform for inflammatory regulation and tissue repair to ameliorate ischemic stroke. *ACS Nano* 2023;**17**:8646−62.
5. Shi YF, Wang Y, Li Q, Liu KL, Hou JQ, Shao CS, et al. Immunoregulatory mechanisms of mesenchymal stem and stromal cells in inflammatory diseases. *Nat Rev Nephrol* 2018;**14**:493−507.
6. Zhao LR, Willing A. Enhancing endogenous capacity to repair a stroke-damaged brain: an evolving field for stroke research. *Prog Neurobiol* 2018;**163**−**164**:5−26.
7. Jin R, Liu L, Zhang SH, Nanda A, Li GH. Role of inflammation and its mediators in acute ischemic stroke. *J Cardiovasc Transl Res* 2013;**6**:834−51.
8. Yang JL, Mukda S, Chen SD. Diverse roles of mitochondria in ischemic stroke. *Redox Biol* 2018;**16**:263−75.
9. Lambertsen KL, Biber K, Finsen B. Inflammatory cytokines in experimental and human stroke. *J Cereb Blood Flow Metab* 2012;**32**:1677−98.
10. Liu SS, Xu JP, Liu YP, You Y, Xie LZ, Tong SQ, et al. Neutrophil-biomimetic "nanobuffer" for remodeling the microenvironment in the infarct core and protecting neurons in the penumbra *via* neutralization of detrimental factors to treat ischemic stroke. *ACS Appl Mater Interfaces* 2022;**14**:27743−61.
11. Zhao ZQ, Zhang XB, Zhang HY, Shan XZ, Bai MY, Wang Z, et al. Elaborately engineering a self-indicating dual-drug nanoassembly for site-specific photothermal-potentiated thrombus penetration and thrombolysis. *Adv Sci* 2022;**9**:e2104264.
12. Zhang Y, Zhang HY, Zhao FQ, Jiang ZP, Cui YL, Ou MT, et al. Mitochondrial-targeted and ROS-responsive nanocarrier *via* nose-to-brain pathway for ischemic stroke treatment. *Acta Pharm Sin B* 2023;**13**:5107−20.
13. Li C, Sun T, Jiang C. Recent advances in nanomedicines for the treatment of ischemic stroke. *Acta Pharm Sin B* 2021;**11**:1767−88.
14. Mittler R. ROS are good. *Trends Plant Sci* 2017;**22**:11−9.
15. Calabrese EJ. Hormesis: path and progression to significance. *Int J Mol Sci* 2018;**19**:2871.
16. Calabrese EJ, Mattson MP, Dhawan G, Kapoor R, Calabrese V, Giordano J. Hormesis: a potential strategic approach to the treatment of neurodegenerative disease. *Int Rev Neurobiol* 2020;**155**:271−301.
17. Gems D, Partridge L. Stress-response hormesis and aging: "that which does not kill us makes us stronger". *Cell Metab* 2008;**7**:200−3.
18. Calabrese EJ, Baldwin LA. Hormesis: the dose-response revolution. *Annu Rev Pharmacol Toxicol* 2003;**43**:175−97.
19. Calabrese EJ, Agathokleous E. Building biological shields *via* Hormesis. *Trends Pharmacol Sci* 2019;**40**:8−10.
20. Takayama Y, Kusamori K, Nishikawa M. Click chemistry as a tool for cell engineering and drug delivery. *Molecules* 2019;**24**:172.
21. Park J, Andrade B, Seo Y, Kim MJ, Zimmerman SC, Kong H. Engineering the surface of therapeutic "living" cells. *Chem Rev* 2018;**118**:1664−90.
22. Xu JP, Zhang YY, Liu YP, You Y, Li FA, Chen Y, et al. Vitality-enhanced dual-modal tracking system reveals the dynamic fate of mesenchymal stem cells for stroke therapy. *Small* 2022;**18**:e2203431.
23. Davalos D, Grutzendler J, Yang G, Kim JV, Zuo Y, Jung S, et al. ATP mediates rapid microglial response to local brain injury *in vivo*. *Nat Neurosci* 2005;**8**:752−8.
24. Nimmerjahn A, Kirchhoff F, Helmchen F, Helmchen F. Resting microglial cells are highly dynamic surveillants of brain parenchyma *in vivo*. *Science* 2005;**308**:1314−8.
25. Kanazawa M, Ninomiya I, Hatakeyama M, Takahashi T, Shimohata T. Microglia and monocytes/macrophages polarization reveal novel therapeutic mechanism against stroke. *Int J Mol Sci* 2017;**18**:2135.
26. Greenhalgh AD, David S, Bennett FC. Immune cell regulation of glia during CNS injury and disease. *Nat Rev Neurosci* 2020;**21**:139−52.
27. Maczurek A, Hager K, Kenklies M, Sharman M, Martins R, Engel J, et al. Lipoic acid as an anti-inflammatory and neuroprotective treatment for Alzheimer's disease. *Adv Drug Deliv Rev* 2008;**60**:1463−70.
28. Haghighatdoost F, Hariri M. The effect of alpha-lipoic acid on inflammatory mediators: a systematic review and meta-analysis on randomized clinical trials. *Eur J Pharmacol* 2019;**849**:115−23.
29. Xu JP, Wang XQ, Yin HY, Cao X, Hu QY, Lv W, et al. Sequentially site-specific delivery of thrombolytics and neuroprotectant for enhanced treatment of ischemic stroke. *ACS Nano* 2019;**13**:8577−88.
30. Lv W, Xu JP, Wang XQ, Li X, Xu QW, Xin HL. Bioengineered boronic ester modified dextran polymer nanoparticles as reactive oxygen species responsive nanocarrier for ischemic stroke treatment. *ACS Nano* 2018;**12**:5417−26.
31. Zhang XL, Zhen XY, Yang YX, Feng Q, Yuan WQ, Xie XY. Precise assembly of inside-out cell membrane camouflaged nanoparticles *via* bioorthogonal reactions for improving drug leads capturing. *Acta Pharm Sin B* 2023;**13**:852−62.
32. Chen J, Ji P, Gnawali G, Chang MY, Gao F, Xu H, et al. Building bioorthogonal click-release capable artificial receptors on cancer cell surface for imaging, drug targeting and delivery. *Acta Pharm Sin B* 2023;**13**:2736−46.
33. Ruan HT, Li YF, Wang C, Jiang YX, Han YL, Li YW, et al. Click chemistry extracellular vesicle/peptide/chemokine nanocarriers for treating central nervous system injuries. *Acta Pharm Sin B* 2023;**13**:2202−18.
34. Du J, Meledeo MA, Wang Z, Khanna HS, Paruchuri VD, Yarema KJ. Metabolic glycoengineering: sialic acid and beyond. *Glycobiology* 2009;**19**:1382−401.
35. Sampathkumar SG, Li AV, Jones MB, Sun Z, Yarema KJ. Metabolic installation of thiols into sialic acid modulates adhesion and stem cell biology. *Nat Chem Biol* 2006;**2**:149−52.
36. Shi W, Li WZ, Zhang JX, Li TH, Song YK, Zeng Y, et al. One-step synthesis of site-specific antibody−drug conjugates by reprograming IgG glycoengineering with LacNAc-based substrates. *Acta Pharm Sin B* 2022;**12**:2417−28.
37. Stansley B, Post J, Hensley K. A comparative review of cell culture systems for the study of microglial biology in Alzheimer's disease. *J Neuroinflammation* 2012;**9**:115.
38. Zheng WW, Zheng XX, Liu SE, Ouyang HS, Levitt RC, Candiotti KA, et al. TNF-α and IL-1β are mediated by both TLR4 and Nod1 pathways in the cultured HAPI cells stimulated by LPS. *Biochem Biophys Res Commun* 2012;**420**:762−7.
39. Su Y, Zhang BL, Sun RW, Liu WF, Zhu QB, Zhang X, et al. PLGA-based biodegradable microspheres in drug delivery: recent advances in research and application. *Drug Deliv* 2021;**28**:1397−418.
40. Kang T, Zhu QQ, Wei D, Feng JX, Yao JH, Jiang TZ, et al. Nanoparticles coated with neutrophil membranes can effectively treat cancer metastasis. *ACS Nano* 2017;**11**:1397−411.
41. Guo JW, Gao XL, Su LN, Xia HM, Gu GZ, Pang ZQ, et al. Aptamer-functionalized PEG-PLGA nanoparticles for enhanced anti-glioma drug delivery. *Biomaterials* 2011;**32**:8010−20.
42. Zhang QZ, Dehaini D, Zhang Y, Zhou JL, Chen XY, Zhang LF, et al. Neutrophil membrane-coated nanoparticles inhibit synovial inflammation and alleviate joint damage in inflammatory arthritis. *Nat Nanotechnol* 2018;**13**:1182−90.
43. Chugh V, Vijaya Krishna K, Pandit A. Cell membrane-coated mimics: a methodological approach for fabrication, characterization for

therapeutic applications, and challenges for clinical translation. *ACS Nano* 2021;**15**:17080−123.
44. Li YY, Zhang JJ. Animal models of stroke. *Anim Model Exp Med* 2021;**4**:204−19.
45. Vorhees CV, Williams MT. Morris water maze: procedures for assessing spatial and related forms of learning and memory. *Nat Protoc* 2006;**1**:848−58.
46. Campbell BCV, De Silva DA, Macleod MR, Coutts SB, Schwamm LH, Davis SM, et al. Ischaemic stroke. *Nat Rev Dis Primers* 2019;**5**:70.
47. Pollock K, Dahlenburg H, Nelson H, Fink KD, Cary W, Hendrix K, et al. Human mesenchymal stem cells genetically engineered to overexpress brain-derived neurotrophic factor improve outcomes in Huntington's disease mouse models. *Mol Ther* 2016;**24**:965−77.
48. Hu XY, Xu YC, Zhong ZW, Wu Y, Zhao J, Wang YC, et al. A Large-scale investigation of hypoxia-preconditioned allogeneic mesenchymal stem cells for myocardial repair in nonhuman primates: paracrine activity without remuscularization. *Circ Res* 2016;**118**:970−83.
49. Ghorbani M, Derakhshankhah H, Jafari S, Salatin S, Dehghanian M, Falahati M, et al. Nanozyme antioxidants as emerging alternatives for natural antioxidants: achievements and challenges in perspective. *Nano Today* 2019;**29**:100775.